Available online at www.sciencedirect.com

ScienceDirect

Ceramics International 40 (2014) 4415–4420

CERAMICS INTERNATIONAL

www.elsevier.com/locate/ceramint

Low hydrothermal temperature synthesis of porous calcium silicate hydrate with enhanced reactivity SiO_2

Wei Guan, Fangying Ji*, Zhuoyao Fang, Dexin Fang, Yong Cheng, Peng Yan, Qingkong Chen

Key Laboratory of Three Gorges Reservoir Region's Eco-Environment, Ministry of Education, Chongqing University, Chongqing 400045, PR China

Received 8 August 2013; received in revised form 25 August 2013; accepted 26 August 2013
Available online 8 September 2013

Abstract

This study presents a novel approach for the synthesis of porous calcium silicate hydrate (CSH) at a low hydrothermal temperature of 110 °C based on enhanced reactivity SiO_2 (i.e. silica/polyethylene glycol (PEG_{2000}) composites) as the source silica material. The as-prepared CSH materials exhibited a porous microstructure with a large number of small mesopores. The porosity formation mechanism of CSH was apparent that cavitation, resulting from sonication, enabled PEG_{2000} (via intercalation on silica) to break apart Si–O–Si structural units, thereby enhancing SiO_2 reactivity at a low hydrothermal temperature. In addition, the presence of PEG_{2000} effectively prevented the aggregation of particles during the formation process of the porous CSH solid. The low temperature synthesis proposed herein represents a viable and effective method for the further development of porous CSH as a functional ceramic material.

Keywords: B. Porosity; D. SiO_2; E. Functional applications; Chemical preparations

1. Introduction

Calcium silicate hydrate (CSH), a functional ceramic material with unique properties of Ca^{2+} and OH^- release, has caused the extensive concern in solving environmental problems caused by the depletion of phosphate resource [1–3]. The large specific surface area of CSH, which is related to its morphology, is the most important factor in its properties to dissolve Ca^{2+} and OH^- [4]. Therefore, consideration of CSH morphology is an important component of efforts to develop highly efficient phosphate recovery material.

Current CSH materials (e.g. Tobermorite, Xonotlite, etc.) used to recover phosphate are prepared using CaO and SiO_2 as the raw material, via dynamic hydrothermal synthesis [5–10]. Unfortunately, the efficiency of phosphate recovery with these materials is limited by: 1) the reactivity of SiO_2 is low at low hydrothermal temperatures, and 2) the residual SiO_2 forms a silicon layer clogging the pore structure of CSH, and subsequently decreasing CSH solubility of CSH [11–15].

In order to enhance the reactivity of SiO_2, current CSH materials have been synthesized at high hydrothermal temperatures (170～220 °C) [16,17]. This high temperature, which is comparable to high pressure (1.6–2.4 MPa), results in a high synthesis cost, and high-energy consumption. Therefore, enhancing the reactivity of SiO_2 is extremely beneficial to form the porous CSH at a low hydrothermal temperature. However, the enhancement of the reactivity of SiO_2 and the porosity formation mechanism of CSH at low hydrothermal temperature are still not completely understood.

In this study, a porous CSH was synthesized at a low hydrothermal temperature (110 °C), using enhanced reactivity SiO_2 as the silica materials. This facile method avoids use of high temperatures, and is an effective method for controlled synthesis of porous CSH. In addition, a novel mechanism for porosity formation of CSH is described herein.

2. Material and methods

2.1. Raw materials

The CaO materials (carbide residue, content of CaO > 75%), and SiO_2 materials (silica, content of SiO_2 > 98%) were

*Corresponding author. Tel./fax: +86 02365127537.
E-mail address: jfytougao@163.com (F. Ji).

0272-8842/$ - see front matter © 2013 Elsevier Ltd and Techna Group S.r.l. All rights reserved.
http://dx.doi.org/10.1016/j.ceramint.2013.08.113

obtained from Chongqing Changshou Chemical Co. Ltd. The chemical composition of the carbide residue and silica are presented in Table 1. PEG_{2000} (the chemical formula is $HO(CH_2CH_2O)_nH$; molecular weight is 2000) was obtained from Chengdu Kelong chemical Co. Ltd. The phosphate solution was prepared by adding KH_2PO_4 (Analytical reagent, Chongqing Boyi Chemical reagent Co. Ltd.) into the solution with initial phosphate concentration of 600 mg/L. These materials and chemicals were stored in sealed bottles.

2.2. Synthesis of silica/PEG_{2000} composites

Prior to CSH synthesis, 39.5 mg of silica and 2 ml of PEG_{2000} (mass fraction of 2%) were dissolved into 300 ml deionized water and sonicated using a ultrasonic generator operating at 100 W (CY-5D, China), and then vigorously agitated in a warm water bath for 48 h at 80 °C to produce a silica/PEG_{2000} composite. These composites were filtered and washed with methanol to removal the excess polymer.

2.3. Hydrothermal synthesis experiments of porous CSH

For the synthesis of CSH samples, silica and silica/PEG_{2000} composites were mixed with CaO material to form a 300 ml slurry (liquid/solid mass ratio is 30/1; Ca/Si molar ratio is 1.75/1). Mixtures were agitated at 90 rpm, and the resulting slurry was put into a high-pressure kettle for hydrothermal synthesis at 110 °C for 6 h. At this low hydrothermal temperature (110 °C), the CSH samples obtained from silica/PEG_{2000} composites and silica were

Table 1
Chemical components of carbide residue.

	Chemical composition (%)									
	CaO	SiO_2	Al_2O_3	SO_2	MgO	Fe_2O_3	SrO	NaOH	CuO	H_2O
Carbide residue	79.34	3.57	2.14	1.22	0.62	0.21	0.26	–	–	12.64
Silica	0.08	97.46	0.16	1.82	–	0.03	–	0.29	0.02	0.14

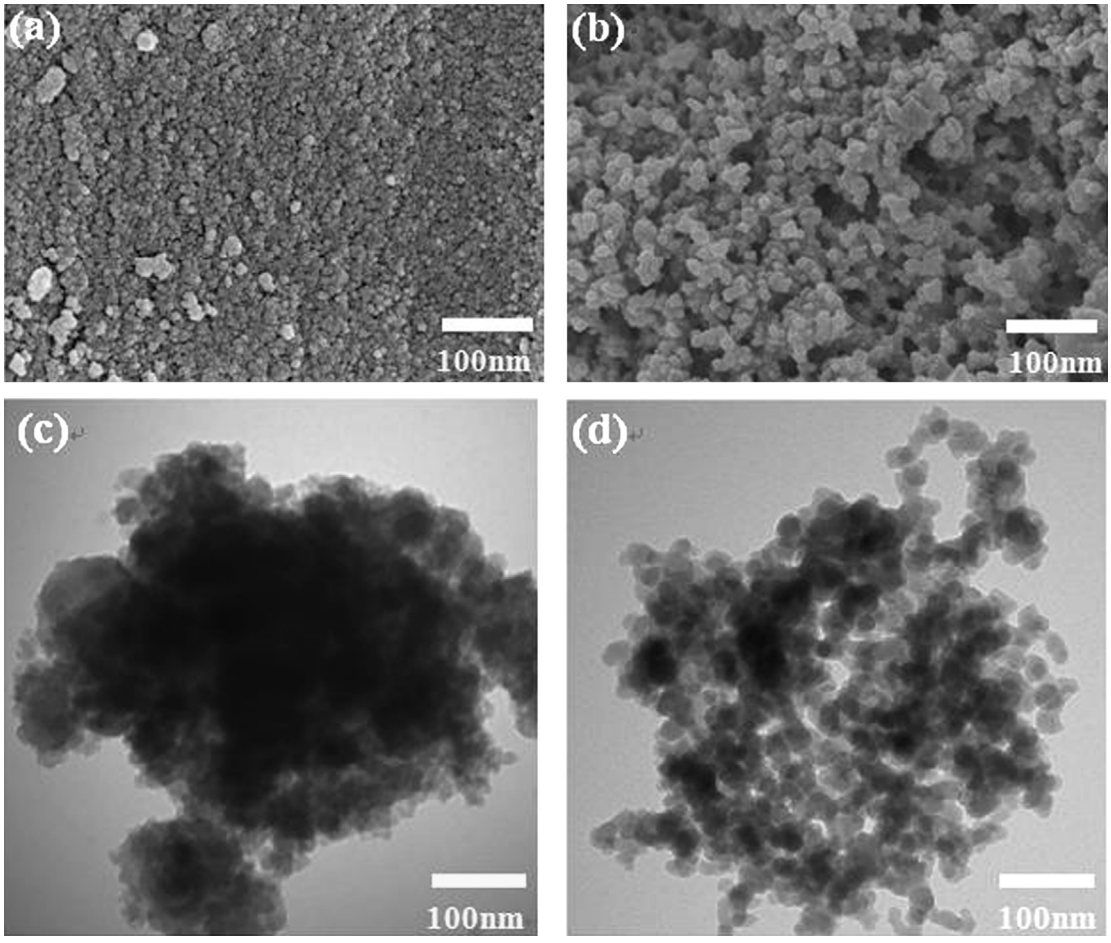

Fig. 1. FESEM photographs of silica (a) and silica/PEG_{2000} (b); TEM images of silica (c) and silica/PEG_{2000} (d).

labeled as CSH (110 °C, silica/PEG_{2000}) and CSH (110 °C, silica), respectively.

2.4. Experiments on phosphate recovery from synthetic solutions

Phosphate recovery properties of the as-prepared CSH samples were investigated in a series of batch experiments. For each one, 1 g/L of synthesized sample was put into the phosphate content solution (the initial phosphate concentration was 600 mg/L) to react for 6 h under given temperature conditions (25 °C). The solid samples after reaction were weighed when separated from the removed synthetic solution and dried at 105 °C. The content of phosphate in the recovered products was identified with atomic absorption spectrophotometry (Atomic Absorption Spectrometer, AA800, USA).

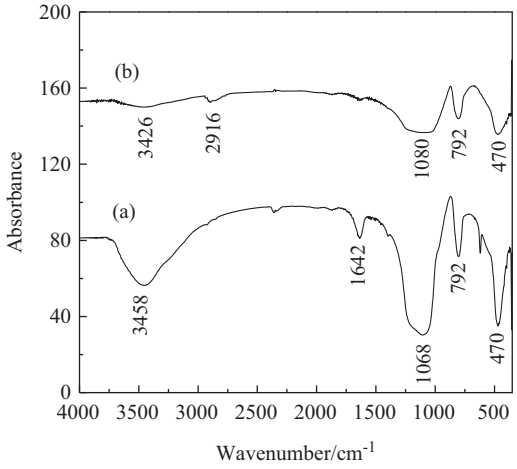

Fig. 2. FI-IR spectra of silica (a) and silica/PEG_{2000} (b).

2.5. Characterization instruments

The phase component and crystal structure was determined by X-ray diffraction at Cu Kα radiation (XRD, model XD-2 instrument, China). The morphology was observed by field-emission scanning electron microscopy (FESEM, IUE, Hitachi, Japan) and transmission electron microscope (TEM, JEOL JEM-2010, Japan). The specific BET surface areas (S_{BET}) and pore structures were observed and nitrogen adsorption–desorption isotherms were plotted on a nitrogen adsorption apparatus (ASAP-2010, USA). The microstructures were characterized by Fourier transformation infrared spectroscopy (FT-IR, IR Prestige-21FT-infrared spectrometer, Shimadzu, Japan).

3. Results and discussion

3.1. Morphological structure of silica/PEG_{2000} composites

The morphology of silica and silica/PEG_{2000} composites was observed by FESEM and TEM (Fig. 1). The original amorphous silica possessed a smooth surface and compact structure (Fig. 1a). In contrast, pore size tended to be larger in the silica/PEG_{2000} composites (Fig. 1b). In addition, compared with the solid structure of the original silica (Fig. 1c), the silica/PEG_{2000} composites possessed hollow microspheres (Fig. 1d). These hollow structures, which were primarily caused by cavitation during sonication, created favorable conditions for the intercalation of PEG_{2000} with silica.

3.2. FT-IR analysis of silica/PEG_{2000} composites

The FT-IR spectrum of the as-prepared samples exhibited absorptions at 3458, 1642, 1068, 792 cm^{-1}, and 470 cm^{-1},

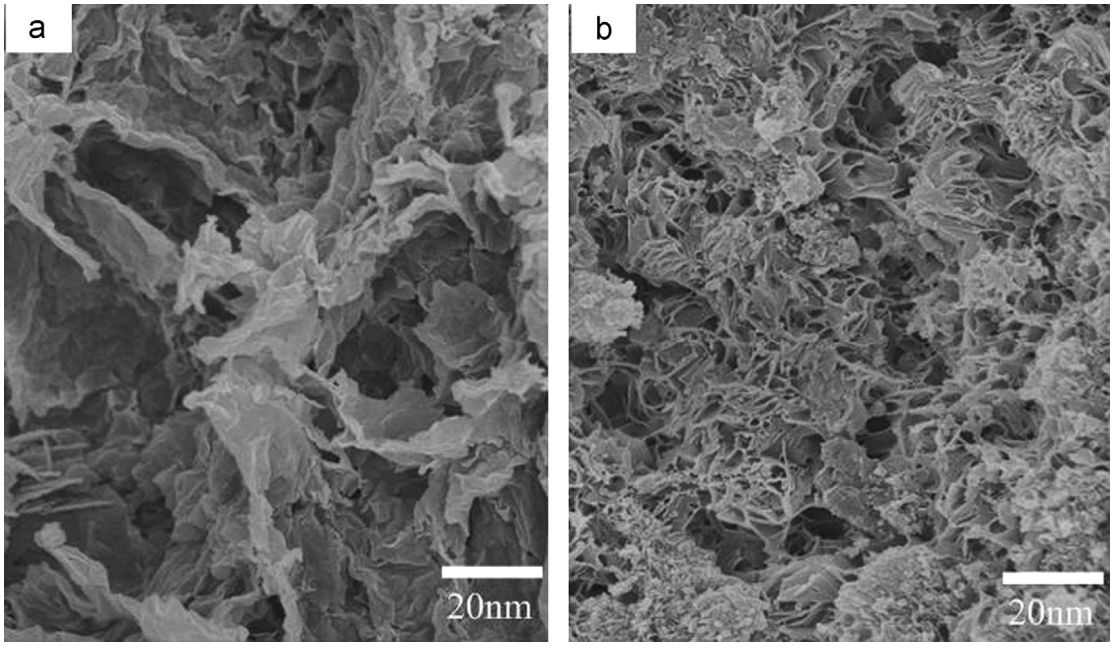

Fig. 3. FESEM photographs of the CSH (110 °C, silica) (a) and CSH (110 °C, silica/PEG_{2000}) (b).

which represent the characteristic absorbance of amorphous SiO_2 (Fig. 2). The band at 3458 cm^{-1} was attributed to the O–H stretching of non-dissociated water molecules, and surface hydroxyls of dissociative chemisorptions [18]. The bands at 1642, 1068, 792, and 470 cm^{-1} were attributed to the stretching vibration of Si–O–Si group of amorphous silica. Because C–O–C stretching oscillation of PEG_{2000} (1080 cm^{-1}) superposed anti-symmetric stretching oscillation of silica (1068 cm^{-1}), Si–O–Si bond was weakened to become a wide peak. The weak Si–O–Si aggregation and easily broken bonds likely resulted in an increase in SiO_2 reactivity. Furthermore, there was no additional peak in silica/PEG_{2000} compared with characteristic absorption peak of silica, except the characteristic absorption peak of PEG_{2000} occurred at about 2916 cm^{-1} due to a bent oscillation peak of C–H bond. These data suggest that there was hydrogen bonding between the surface of silica and PEG_{2000} molecules, causing adsorption of PEG_{2000} on the silica surface.

3.3. The morphology and pore structure of CSH

As evident in the representative micrographs, CSH (110 °C, silica) possessed a dense pore structure with large mesopores (Fig. 3a). For CSH (110 °C, silica/PEG_{2000}) (Fig. 3b), a porous microstructure developed with a large number of small mesopores. The thickness of the nanoscale layers of CSH (110 °C, silica) and CSH (110 °C, silica/PEG_{2000}) was 15.3–21.5 nm and 27.4–31.2 nm, respectively.

The specific BET surface areas (S_{BET}) and pore structure of the prepared samples were investigated using adsorption–desorption measurements. As shown in Table 2, the S_{BET} of CSH (110 °C, silica/PEG_{2000}) increases to 168 m^2/g, compared to CSH (110 °C, silica) (65 m^2/g). The pore volume of CSH (110 °C, silica/PEG_{2000}) increases to 0.87 cm^3/g, compared to CSH (110 °C, silica) (0.23 cm^3/g). A greater specific surface area and pore volume of CSH lead to an enhancement of capabilities of the release of Ca^{2+} and OH^-. Thus, the large S_{BET} and pore volume of CSH samples may play a role in enhancing the phosphate recovery property.

Table 2
Specific BET surface areas and pore parameters of CSH samples.

CSH samples	Total volume (cm^3/g)	Peak pore diameter (nm)	S_{BET} (m^2/g)
CSH (110 °C, silica)	0.23	20.35	65
CSH (110 °C, silica/PEG_{2000})	0.87	8.74	168

Fig. 4a shows the N_2 adsorption–desorption isotherms of the as-prepared CSH samples. According to the Brunauer–Deming–Deming–Teller (BDDT) classification, the majority of physisorption isotherms can be grouped into six types. The isotherms of all the samples belong to type IV, including the pore-size distributions in the mesoporous regions. The shapes of hysteresis loops are of the type H3, which is associated with mesopores formed due to aggregation of plates-like particles [19,20].

Pore size distributions of as-prepared CSH samples are revealed in Fig. 4b. The pore size distribution curves of CSH (110 °C, silica) are bimodal with smaller (~2.87 nm) and larger (~48.54 nm) mesopores. In contrast, the pore size distribution of CSH (110 °C, silica/PEG_{2000}) is classified into small mesopores (~8.74 nm) range. The small mesopores and larger ones came from the aggregation of primary particles and secondary particles, respectively. This result indicated that the small pore size distribution resulted in the large S_{BET}.

3.4. Phase structure of CSH

The XRD pattern of CSH (110 °C, silica) shows clear characteristic SiO_2 peaks at $2\theta = 8.414°$, 20.305°, 21.562°, 35.553°, 38.696°, 43.938°, and 52.714°, which are ascribed to the diffraction of (001), (100), (101), (102), (110), (103), (004), and (132) planes, indicating silica did not participate in the formation of CSH efficiently at a low hydrothermal temperature (Fig. 5a). In contrast, the XRD patterns of CSH (110 °C, silica/PEG_{2000}), instead of the characteristic SiO_2 peaks, exhibited characteristics peaks of Jennite (PDF card 18-1206, chemical formula $Ca_9Si_6O_{18}(OH)_6 \cdot 8H_2O$) which is ascribed to the diffraction of (002), (102) and (301) planes (Fig. 5b). In addition, the crystallinity of CSH (110 °C, silica/

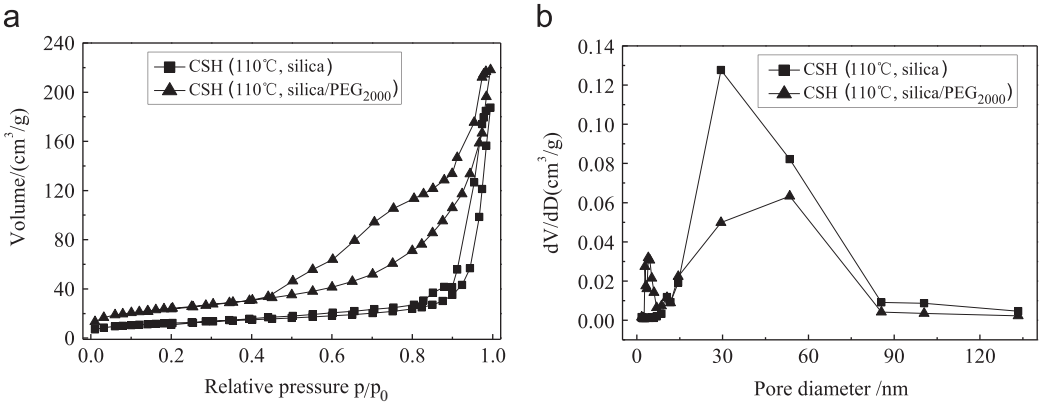

Fig. 4. N_2 adsorption–desorption isotherms (a) and pore-size distribution curves (b) of the as-prepared CSH samples.

PEG_{2000}) declined obviously due to the fact that the PEG_{2000} was inserted into the interlamination of CSH to increase the interlayer interval. Furthermore, the increased d_{002} spacing was due to the polymers included into the pore structure of CSH (110 °C, silica/PEG_{2000}); indicating PEG treatments induced structural rearrangement of CSH resulting from partial intercalation or expansion.

3.5. The porosity formation mechanism of CSH

The schematic illustration of the porosity formation process of CSH is shown in Fig. 6. The porosity formation mechanism of CSH involved PEG_{2000} intercalation into silica, breaking the Si–O–Si bond. Doing so enabled for greater interaction between $H_3SiO_4^-$ (generated by silica/PEG_{2000} composites) and Ca^{2+} and OH^- (generated by carbide residue). In addition, the water content within the CSH structure is likely reduced as H_2O molecules are replaced by hydrated PEG_{2000} [21]. Therefore, the presence of PEG_{2000} prevented particle aggregation during the formation process of the CSH solid. This porous structure, lacking a silicon layer that would otherwise clog the pore structure is beneficial to the release of Ca^{2+} and OH^-.

3.6. The enhanced phosphate recovery property of CSH

Fig. 7 shows the XRD patterns of the phosphate products recovered by CSH (110 °C, silica) (Fig. 7a) and CSH (110 °C, silica/PEG_{2000}) (Fig. 7b), respectively. The characteristic peaks of HAP (PDF card 09-0432, chemical formula $Ca_5(PO_4)_3(OH)$) with different strength can be detected in these two products. The sharp dominant peaks of HAP obtained by CSH (110 °C, silica/PEG_{2000}) at (002) and (211) lattice plane were stronger than those of the other, indicating that the HAP crystal produced better on the surface of CSH (110 °C, silica/PEG_{2000}) by comparison. The phosphate content of the product recovered by CSH (110 °C, silica/PEG_{2000}) increased to 123.5 mg/g, compared with CSH (110 °C, silica) (93.4 mg/g). This result indicated that CSH with high phosphate recovery properties can be synthesized at low hydrothermal temperature. Meanwhile, the recovered phosphate product HAP, due to its abundant phosphate content, can be reused as phosphate rock or phosphate fertilizer. Therefore, the as-prepared porous CSH, as a functional ceramic material, has potential application for use in the recovery of phosphate from wastewater, further reducing the negative environmental effects of continual natural phosphate resource depletion.

4. Conclusions

In summary, this study demonstrates the successful syntheses of CSH (with a porous structure) under lower than usual hydrothermal conditions (110 °C). The as-prepared CSH materials exhibited a porous microstructure with a large number of small mesopores. The porosity formation mechanism in this process mainly involved the following:

I The reactivity of SiO_2 was enhanced due to the intercalation of PEG_{2000} as a result of sonication, thus the silica/PEG_{2000} composite participated in the efficient formation of CSH at a low hydrothermal temperature.

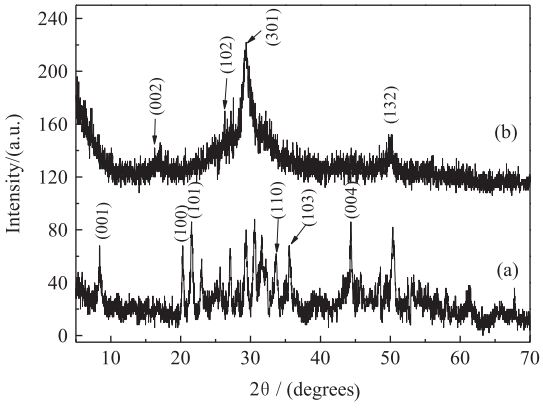

Fig. 5. XRD patterns of CSH (110 °C, silica) (a) and CSH (110 °C, silica/PEG_{2000}) (b).

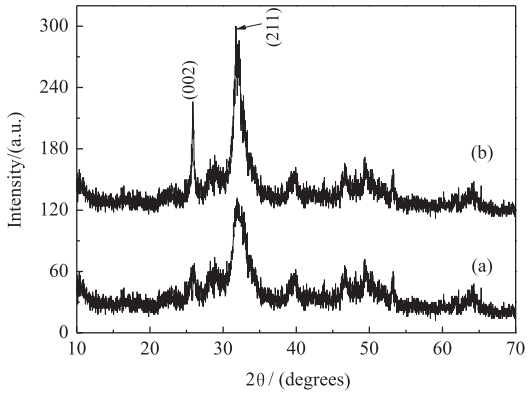

Fig. 7. XRD patterns of phosphate product recovered by CSH (110 °C, silica) (a) and CSH (110 °C, silica/PEG_{2000}) (b).

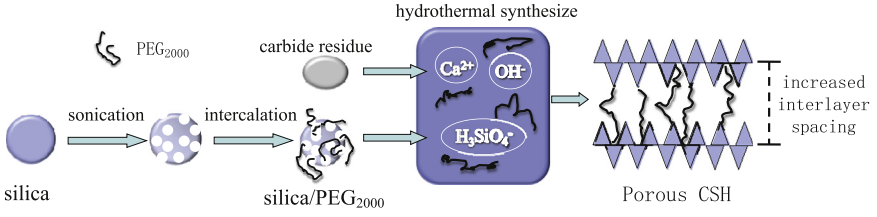

Fig. 6. Schematic illstration of the porosity formation process of CSH.

II The presence of PEG_{2000} effectively prevented the aggregation of particles during the formation process of the CSH solid.

This low hydrothermal temperature synthesis condition proposed herein represents a viable and effective method for the further development of CSH as a functional ceramic material. This porous CSH has potential application for use in the recovery of phosphate from wastewater, further reducing the negative environmental effects of continual natural phosphate resource depletion.

References

[1] P.A. Mouthuy, A. Crossley, H. Ye, Fabrication of calcium phosphate fibers through electrospinning and sintering of hydroxyapatite nanoparticles, Materials Letters 106 (2013) 145–150.

[2] Y.H. Song, D. Donnert, U. Berg, G.W. Peter, R. Nueesch, Seed selections for crystallization of calcium phosphate for phosphorus recovery, Journal of Environmental Sciences 19 (2007) 591–595.

[3] Y.H. Song, G.W. Peter, U. Berg, R. Nueesch, D. Donnert, Calcite-seed crystallization of calcium phosphate for phosphorus recovery, Chemosphere 63 (2006) 236–243.

[4] D. Sugiyama, T. Fujita, A Thermodynamic model of dissolution and precipitation of calcium silicate hydrates, Cement and Concrete Research 36 (2006) 227–237.

[5] W. Guan, F.Y. Ji, Q.K. Chen, P. Yan, Q. Zhang, Preparation and phosphorus recovery performance of porous calcium-silicate-hydrate, Ceramics International 39 (2013) 1385–1391.

[6] O. Kenji, U. Maasahide, K. Jumpei, M. Keiichi, A. Tsuyoshi, T. Masaya, et al., Novel technique for phosphorus recovery from aqueous solutions using amorphous calcium silicate hydrates (A-CSHs), Water Research 47 (2013) 2251–2259.

[7] I.G. Richardson, Tobermorite/jennite- and tobermorite/calcium hydroxide-based models for the structure of C-S-H: applicability to hardened pastes of tricalcium silicate, β-dicalcium silicate, Portland cement, and blends of Portland cement with blast-furnace slag, metakaolin, or silica fume, Cement and Concrete Research 34 (2004) 1733–1777.

[8] A. Renman, G. Renman, Long-term phosphate removal by the calcium-silicate material Polonite in wastewater filtration systems, Chemosphere 79 (2010) 659–664.

[9] S.U. Sezen, S.R.C. Sejung, C.J. Benmore, H.R. Wenk, Compositional evolution of calcium silicate hydrate(C-S-H) structures by total X-ray scattering, Journal of the American Ceramic Society 2 (2012) 793–798.

[10] M.Q. Li, H.X. Liang, Formation of micro-porous spherical particles of calcium silicate (xonotlite) in dynamic hydrothermal process, China Particuology 3 (2004) 124–127.

[11] K. Kong, K. Giichiro, K. Koichi, B.C. Sung, K. Masanobu, O. Chikara, Preparation of bioactive spherical particles in the $CaO–SiO_2$ system through sol–gel processing under coexistence of poly(ethylene glycol), Journal of the European Ceramic Society 28 (2008) 1595–1602.

[12] H.Y. Chang, C.W. Thangamuthu, Lin, Structure–property relationships in PEG/SiO_2 based proton conducting hybrid membranes—a ^{29}Si CP/MAS solid-state NMR study, Journal of Membrane Science 228 (2004) 217–226.

[13] R. Zhao, B.L. Su, Self-assembly of phosphorylated poly(ethyleneimine) for use as biomimetic templates in the formation of hybrid hollow silica spheres, Materials Letters 74 (2012) 163–166.

[14] A.A.P. Mansur, H.S. Mansur, Preparation, characterization and cytocompatibility of bioactive coatings on porous calcium-silicate-hydrate scaffolds, Materials Science and Engineering C 30 (2010) 288–294.

[15] I. Baur, K. Peter, D. Mavrocordatos, B. Wehrli, C.A. Johnson, Dissolution-precipitation behaviour of ettringite, monosulfate, and calcium silicate hydrate, Cement and Concrete Research 34 (2004) 341–348.

[16] W.J. Zhu, Y. Zhou, W.H. Ma, M.M. Li, J. Yu, K.Q. Xie, Using silica fume as silica source for synthesizing spherical ordered mesoporous silica, Materials Letters 92 (2013) 129–131.

[17] W. Guan, F.Y. Ji, Q.K. Chen, P. Yan, W.W. Zhou, Influence of hydrothermal temperature on phosphorus recovery efficiency of porous calcium silicate hydrate, Journal of Nanomaterials 9 (2013) 1–6.

[18] Q. Guo, T. Wang, Influence of SiO_2 pore structure on phase change enthalpy of shape-stabilized polyethylene glycol/silica composites, Journal of Materials Science 48 (2013) 3716–3721.

[19] F. Dong, Y.J. Sun, M. Fu, Z.B. Wu, S.C. Lee, Room temperature synthesis and highly enhanced visible light photocatalytic activity of porous BiOI/BiOCl composites nanoplates microflowers, Journal of Hazardous Materials 219–220 (2012) 26–34.

[20] F. Dong, Y.J. Sun, M. Fu, W.K. Ho, S.C. Lee, Z.B. Wu, Novel in situ n-doped $(BiO)_2CO_3$ hierarchical microspheres self-assembled by nanosheets as efficient and durable visible light driven photocatalyst, Langmuir 28 (2012) 766–773.

[21] J. Ha, S. Chae, K.W. Chou, T. Tyliszczak, P.J.M. Monteiro, Effect of polymers on the nanostructure and on the carbonation of calcium silicate hydrates: a scanning transmission X-ray microscopy study, Journal of Materials Science 47 (2012) 976–989.